Chapter 2

"Heart" of Solid State Hydrogen Storage

"I believe that one day Hydrogen and Oxygen,
Which together form water, will be used either alone
Or together as an inexhaustible source of heat and light"
– Jules Verne (1874)

Abstract

This chapter explains the basic concept of solid state hydrogen storage. The reaction between gas phase hydrogen and a metal surface are illustrated using the one–dimensional Lennard–Jones potential of atomic H and molecular H_2. The formation of metal hydrides can be divided into the five elementary reactions, such as physisorption, dissociation of hydrogen molecules, surface penetration, diffusion and hydride formation, which is also explained. Based on the literature survey, state–of–the art report of most popular metallic hydrides (elemental, AB, A_2B, AB_2, and AB_5 type) is briefly presented. The computational formalism of absorbed/desorbed mass % of hydrogen using ideal gas law is explained. Computation of deviations due to departure from idealism using three different equations of state for real gases is also presented. These equations are the Van–der–Waal, Redlich–Kwong and Redlich–Kwong–Soave equation, respectively. The reaction kinetics of the solid state hydrogen storage materials using different kinetics models, namely, first order model, shrinking core model, and Johnson–Mehl–Avrami model is also studied. Finally, explanations are presented on methods of predicting thermodynamic properties (ΔH and ΔS) of the metallic hydrides using the pressure composition isotherm curve method and Van't Hoff relationship.

2.1 Introduction

There are few major ways of storing hydrogen (gaseous storage, liquid hydrogen storage and metal hydride storage). Due to deficiencies of the less volume, weight and losses involved in these storage modes, metal hydrides can be considered as the best way of storing atomic hydrogen. Storing it as metal hydrides seems to be the most cost efficient way. The metal–hydrogen system consists of a metallic material, hydrogen gas and an interface region between them. As the name implies the metal react with hydrogen under certain parameters and gives solid solution of metal and hydrogen. This material is known as metal hydride [1]. However, they exhibit, when exposed to hydrogen at certain pressure and temperatures. They absorb large quantities of hydrogen and form metal hydrogen compounds. When this happens, hydrogen is distributed compactly throughout the metal lattice.

$$\text{Metal} + \text{Hydrogen} \underset{\text{Temperatures}}{\overset{\text{Certain pressures}}{\longleftrightarrow}} \text{Metal Hydride} \pm \text{Heat} \quad \text{---------- (2.1)}$$

Or, in symbolically,

$$M + \frac{x}{2} H_2 \leftrightarrow MH_x \qquad (\alpha\text{–phase}) \qquad \text{---------- (2.2)}$$

$$MH_x + \frac{y-x}{2} H_2 \leftrightarrow MH_y \qquad (\beta\text{–phase}) \qquad \text{---------- (2.3)}$$

The double–headed arrow indicates that the reaction is reversible and exists as an equilibrium state. In other words, by changing conditions, the reaction can be made to go in either the forward or reverse directions. The heat on the right-hand side indicates that heat or energy is released, when the metal hydride is formed. Thus, heat must be put into the system to release hydrogen from the metal hydride phase. The heat is the enthalpy (heat of formation) of the reaction and is an indication of the strength of the metal-hydrogen bond in the metal hydride phase. Hydrogen gas adsorbs onto the interface region. At the interface, the molecule is disassociated into individual hydrogen atoms that are able to absorb or dissolve into the metal phase

(Fig. 2.1) [2]. The random dissolution of hydrogen atoms in the metal phase is known as the α–phase. Within the metallic phase, the hydrogen atoms can start to arrange themselves in a specific configuration with the metal atoms, forming the metal hydride phase, called the β–phase [3].

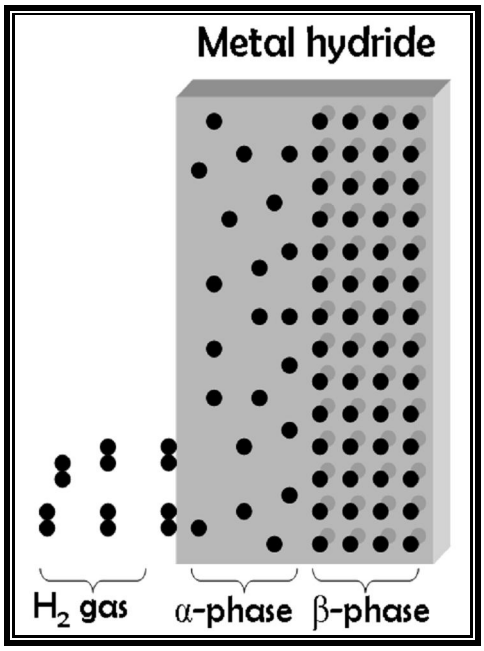

Fig. 2.1: Pictorial view of metal hydride

Metal hydrides represent an exciting new method of storing hydrogen. Thus, metal hydride can be used in power system applications and also, can be used in mobile applications; like power cars, power boats, buses, etc… Since, the absorption and desorption of hydrogen by metal hydrides are exothermic and endothermic reactions, respectively. Metal hydrides can also be used for generating and/or absorbing of heat. Thus cooling and/or heating are produced by the reversible reactions between hydrogen gas and a pair of metal alloys.

2.2 Basic Concept on Metallic Hydride

The reaction between gas phase H_2 and a metal surface are schematically illustrated in Fig. 2.2, where the one-dimensional Lennard–Jones potential of atomic H (dotted line) and molecular H_2 is shown (solid line) [4, 5]. Using this potential, the basic concepts of metallic hydrides can be explained as following:

Far from the surface the two lines are separated by the hydrogen dissociation energy, which is 218 kJ/mol H_2. A H_2 molecule moving towards the surface will at some point feel a weak attractive force in the range of approximate 0–20 kJ/mol H_2 (Van–der–Waals forces). It is corresponding to molecular physisorption [6].

If the molecule is moved closer to the surface, the potential energy will increase due to repulsion. At some point, the potential energy of the H_2 molecule will intersect with the potential energy of the H atom. After this point, it is energetically more favorable for the two H atoms to be separated and bonded to the metal surface, rather than bonded to each other. Hence dissociation will occur. At this intersection, the potential energy is larger than zero relative to gas phase H_2 dissociation. It is said to be activated and the height of potential determines the activation barrier.

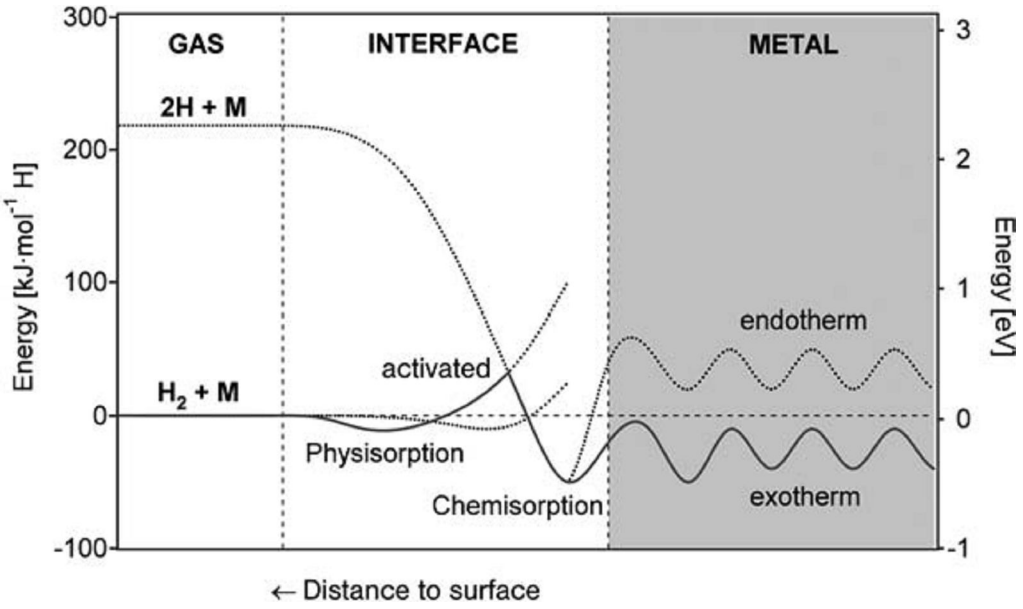

Fig. 2.2: Schematic Lennard – Jones potential energy diagram

If the intersection is located at approximate zero potential energy, dissociation is said to be non-activated. In the former case, only the fraction of H_2 molecules (with energy larger than the activation barrier) will be able to dissociate. After dissociation, the H atoms find minimum potential energy, which correspond to the H atoms being bonded to the metal surface [7, 8]. It is shown as chemisorptions (~ 50 kJ/mol H_2). If

the H–M bond is stronger than the H–H bond, chemisorptions is said to be exothermic. Likewise, if the H–H bond is the strongest, chemisorptions is said to be endothermic.

Beyond the point of chemisorptions, the H–atoms can penetrate the first metal atomic layer into the subsurface through an activated process. In this process, it can diffuse into the bulk (as a solid solution) of the metal and the hydrogen atoms contribute with their electron to the band structure of the metal. If the potential energy of bulk H–atoms is below zero relative to gas phase H_2, hydrogen solid solution is said to exothermic. If the potential energy of bulk H–atoms is above zero, hydrogen solid solution is said to be endothermic.

2.3 Reaction Mechanism of the Solid State Hydrogen Storage

The exposure of certain metals and alloys to hydrogen under appropriate pressure and temperature conditions results in the formation of a hydride layer on the sample's surface. Hydrogen gas is adsorbed on the surface of the sample and transferred through the layer in diffusion like process, down to the reaction site, where metal to hydride transformation occurs. A schematic visualization of the interaction of hydrogen with a metal is described in Fig. 2.3 [9]. Fig. 2.2 is showed an energy representation, where as Fig. 2.3 shows all the individual reaction steps including bulk processes. For each step transmitting hydrogen into the sample, there is a reverse process releasing hydrogen back to the gas phase. The reaction rate is given by the net absorption flow of hydrogen into the surface layer. There are five main sequential steps [10–12]:

(i) Physisorption of hydrogen molecules
(ii) Dissociation of hydrogen molecules and chemisorption
(iii) Surface penetration of hydrogen atoms
(iv) Diffusion of hydrogen atoms through the hydride layer
(v) Hydride formation at the metal/hydride interface

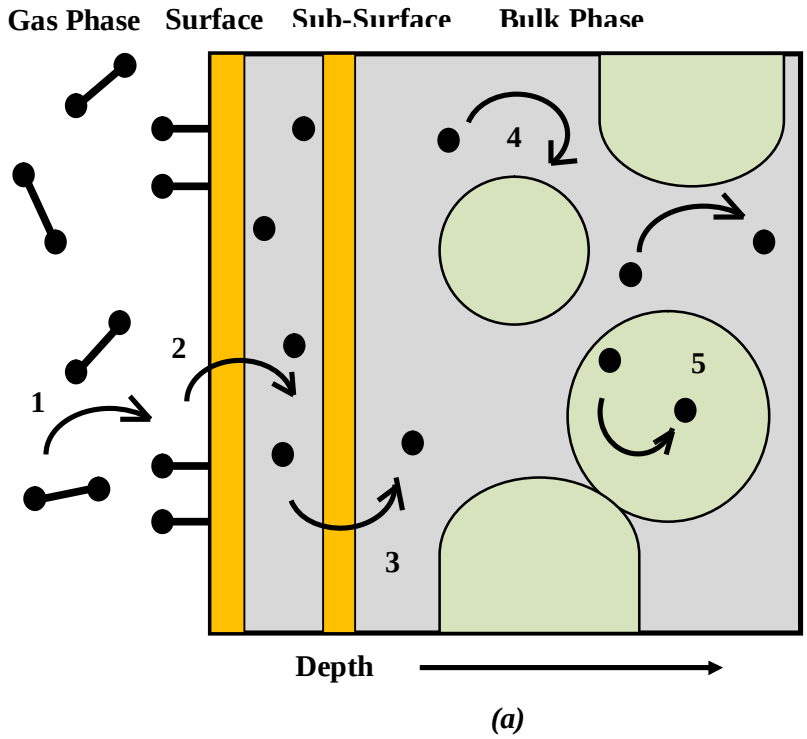

(a)

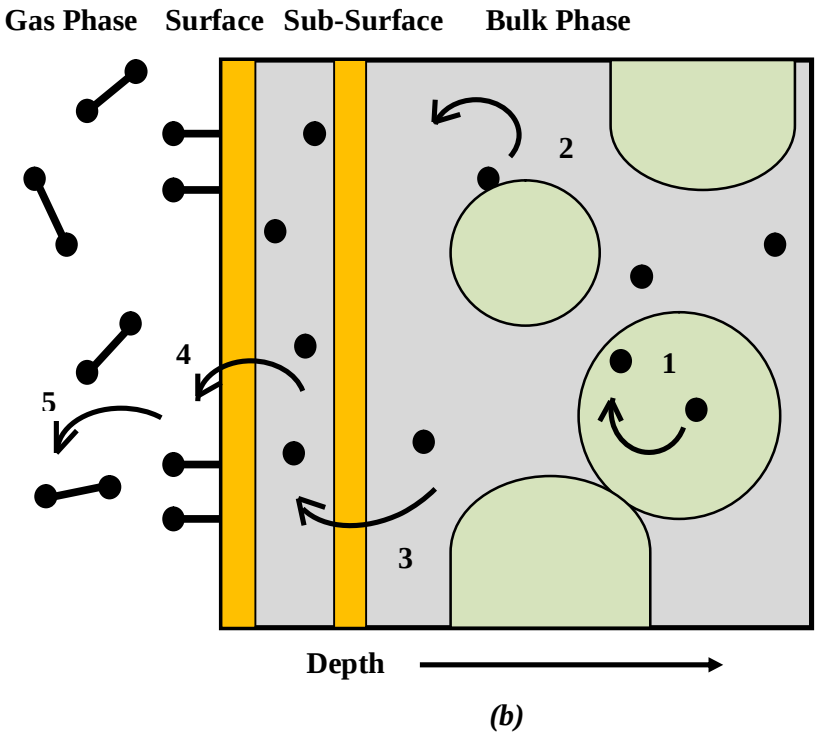

(b)

Fig. 2.3: Schematic mechanisms illustration of the different involved in the formation of a metal hydride: (a) Absorption mechanism and (b) Desorption mechanism

One of the steps (i) to (v) will be much slower than all others and is therefore rate determining. All other reaction steps are in equilibrium. The steady state condition requires that the change in concentrations of intermediate species. For example, the concentration of physisorbed hydrogen molecules is small, when compared with the reaction rate of hydrogen formation. The activity of hydrogen at positions before and after, the rate determining step can then be expressed by equilibrium relations.

(i) Physisorption

The physisorption reaction is given by,

$$H_{2(gas)} + \square_{(ph)} \longrightarrow H_{2(ph)} \quad \text{---------- (2.4)}$$

Where, $\square$ denotes an empty physisorption site on the surface. This reaction shows in Fig. 2.3(a) (point 1). Since physisorption of gas molecules on surfaces requires almost no activation energy. The impact rate of the hydrogen molecules on the surface is very large at higher pressures. The gas phase is certainly in equilibrium with the physisorbed state and it is not a rate determining state.

(ii) Chemisorption

The next reaction partial step is dissociation of the H_2 molecules and chemisorption of hydrogen atoms on the surface of the hydride, given by the reaction (see Fig. 2.3(a) point 2),

$$H_{2(ph)} + 2\,\square_{(ch)} \longrightarrow 2H_{(ch)} + 2\,\square_{ph)} \quad \text{---------- (2.5)}$$

Where, $\square$ denotes an empty chemisorption site on the surface. The rate of a reaction is given by the reaction rate in the forward direction minus the reaction rate in the backward direction. The reaction rates in the forward and backward directions are given as a product of the concentration of the reacting species multiplied by a rate constant. It is assumed that enough vacant chemisorption and physisorption sites are available for the forward and backward reactions. If chemisorption is the rate determining step, the concentration of the physisorbed hydrogen molecules can be given as a function of the hydrogen pressure. The concentration of chemisorbed

hydrogen atoms can be expressed in terms of the decomposition or plateau pressure of the hydride phase.

(iii) Surface Penetration

The transfer of chemisorbed hydrogen on the surface to the first subsurface layer in the hydride can be considered as a single diffusion jump. But, its activation energy is different from the diffusion in bulk of hydride. Therefore, it is necessary to formulate this step separately. Diffusion of hydrogen is assumed here to take place by a vacancy mechanism of hydrogen in hydride lattice. The surface penetration process is described by,

$$H_{(ch)} + \square_{\beta(r0)} \longrightarrow \square_{(ch)} \qquad \text{---------- (2.6)}$$

Where, $\square_{\beta(r0)}$ denotes a vacancy in the lattice of the β phase just below the surface. This reaction shows in Fig. 2.3(a) (point 3).

(iv) Diffusion

The next reaction partial step is the diffusion of hydrogen atoms from the subsurface through hydride layer to the α/β interface. This reaction mechanism shows in Fig. 2.3(a) (point 4).

(v) Hydride Formation

The final reaction step is formation of hydride at the metal/hydride interface. The vacancy mechanism is considered for this reaction (see Fig. 2.3(a) point 5). The reaction is given by,

$$M_{(r\alpha)} \longrightarrow \square_{\beta(r\alpha)} + MH \qquad \text{---------- (2.7)}$$

The hydrogen desorption process can be explained reverse way of absorption. The α–phase is formed first at the metal/gas interface of the spherical particles according to Fig. 2.3(b). Again, five reaction partial steps are required for the overall reaction [13]:

(i) Hydride decomposition at the hydride / metal interface

(ii) Diffusion of hydrogen atoms through the α phase

(iii) Surface penetration of hydrogen atoms

(iv) Recombination of chemisorbed hydrogen atoms and physisorption

(v) Desorption to the gas phase

(i) Hydride Decomposition

The first reaction partial step for the desorption process is decomposition of the hydride at the metal hydride interface and formation of the α–phase. In the α–phase, hydrogen atoms are dissolved as interstitials. The reaction is thus given by,

$$MH + \square_{\alpha(r\beta)} \longrightarrow H_{\alpha(r\beta)} + M \quad \text{---------- (2.8)}$$

Where, $\square_{\alpha(r\beta)}$ represents an empty interstitial site in the α–phase at the α/β interface. This reaction shows in Fig. 2.3(b) (point 1).

(ii) Diffusion

The diffusion can be explained same as per absorption mechanism, but the direction is reverse with respect to absorption. The diffusion mechanism here is diffusion of interstitials and not of vacancies. This reaction shows in Fig. 2.3(b) (point 2).

(iii) Surface Penetration

The step from the last interstitial site inside the α–phase to the surface is given by (see the Fig. 2.3(b) (point 3)),

$$H_{\alpha(r0)} + \square_{(ch)} \longrightarrow H_{ch} + \square_{\alpha(r0)} \quad \text{---------- (2.9)}$$

Where, $\square_{(ch)}$ denotes empty chemisorption sites and $\square_{\alpha(r0)}$ empty subsurface interstitial sites.

(iv) Recombination

The next reaction partial step is the recombination of chemisorbed hydrogen atoms and formation of physisorbed hydrogen molecules on the surface;

$$2H_{ch} + \square_{(ph)} \longrightarrow H_{2(ph)} + 2\,\square_{(ch)} \quad \text{---------- (2.10)}$$

This reaction shows in Fig. 2.3(b) (point 4).

(v) Desorption to the Gas Phase

The final reaction partial step is desorption of physisorbed molecules to the gas phase. It is not considered as a rate determining step, because of the low activation energies involved. This shown by (see the Fig. 2.3(b) (point 5)),

$$H_{(ph)} \longrightarrow H_{2(g)} \quad \text{---------- (2.11)}$$

2.4 A State–of–the Art Report of Most Popular Metallic Hydride

Metal hydride systems have wide ranging applications such as: hydrogen storage, energy storage, hydrogen compressor, pumping, cooling, heating and heat transformation systems, rechargeable batteries, sensing devices, hydrogen purification etc. In this chapter, a detailed state–of–the art report of metal hydride characterization and technology for stationary and mobile applications are presented. This is followed by studies on morphology, structural analysis, storage capacity and kinetics of metal hydride.

2.4.1 Element

The alkali metals, group I of the periodic table of the elements are formed hydrides with a high degree of ionic bonding character. Moreover, the electrons are localized around the atom nuclei. Thus, the bonding between hydrogen and metal is strong, resulting in high decomposition temperatures. The alkaline metals are light elements (low density), which crystallize in a body centered cubic (bcc) arrangement. Due to their low melting points, the hydrides of the alkali metals decompose into hydrogen and pure metal above the melting point of the metal. Selected properties of the alkali metal hydrides are compiled in Table–2.1 [14, 15].

Table–2.1: Properties of the alkali metal hydrides

Properties	Alkali Metal Hydrides				
	LiH	**NaH**	**KH**	**RbH**	**CsH**
Hydrogen storage capacity, mass%	12.7	4.2	2.5	1.2	0.8
Metal density, gm/cm^3	0.535	0.971	0.862	1.532	1.886
Metal hydride density, gm/cm^3	0.769	1.36	1.43	2.59	3.41
Melting temperature, °C	181	98	36	39	28
Desorption temperature, °C	720	420	417	170	170

The alkaline earth metal hydride, BeH_2 is a mostly covalent bonding character, whereas ionic hydrides are CaH_2, SrH_2, and BaH_2. In between, MgH_2 is with a more complex bonding character. Generally, the electronic density is located around the atoms with a net charge of Mg close to (+2) and negatively charged H atoms with a charge of (– 0.94) to (– 0.26). The remaining electron density is distributed evenly in the interstitial region. Although, recent experiments have revealed regions with increased electron density between Mg and H atoms, clearly suggesting that it has a partial covalent bonding character. Both Beryllium and Magnesium crystallize in the hexagonal close packed (hcp) structure, but transforms into an orthorhombic structure and a tetragonal structure, respectively, for the corresponding hydrides. The hydrides of the alkaline earth metals are insulators with band gaps in the range of 3 to 6 eV for Be Mg and Ca. The alkaline earth metal hydrides are quite stable and require high temperatures for decomposition. Selected properties of the alkaline earth metal hydrides are compiled in Table–2.2 [16–18].

Table–2.2: Properties of the alkaline earth metal hydride

Properties	Alkaline earth metal hydrides				
	BeH_2	**MgH_2**	**CaH_2**	**SrH_2**	**BaH_2**
Hydrogen storage capacity, mass%	18.3	7.66	4.8	2.2	1.4
Metal density, gm/cm^3	1.85	1.74	1.54	2.64	3.62
Metal hydride density, gm/cm^3	0.65	1.45	1.7	3.26	4.18
Melting temperature, °C	1287	650	842	777	727
Desorption temperature, °C	250	330	600	675	675

Compared to the hydrides of the main group I and II elements, the transition metal hydrides have much more diverse physical properties. The hydrides formed by the early transition metals are generally very stable (TiH_2 requires heating to above 450 °C for decomposition) and moving to right the hydrides become less stable. Around the middle of the transition metals (Mn, Fe) the stability goes through a local minimum. Another major difference between transition metal hydrides and the hydrides of main group I and II is the fact that the bonding character in transition metals is metallic. The $PdH_{0.6}$ has an excellent reversible kinetics at ambient conditions, but it has hydrogen storage capacity only 0.6 mass% and very costly [19]. The $VH_{0.9}$ – VH_2 has also reversible hydrogen storage capacity up to 2.08 wt% at ambient conditions [20].

Mg and its Engineering Properties: If metal hydrides are to become important energy carriers in mobile vehicles, the total mass of the storage system needs to be reduced. A very promising candidate is Magnesium for mass sensitive applications. The metallic Mg has hexagonal crystal structure with lattice parameters a = 3.2094 Å and c = 5.2108 Å. The β−MgH_2 is tetragonal (see Fig. 2.4), with lattice parameters a = 4.517 Å and c = 3.0205 Å [21]. There is another type of Magnesium hydride (γ−MgH_2 phase), but it is unstable and exists only under high hydrogen pressure.

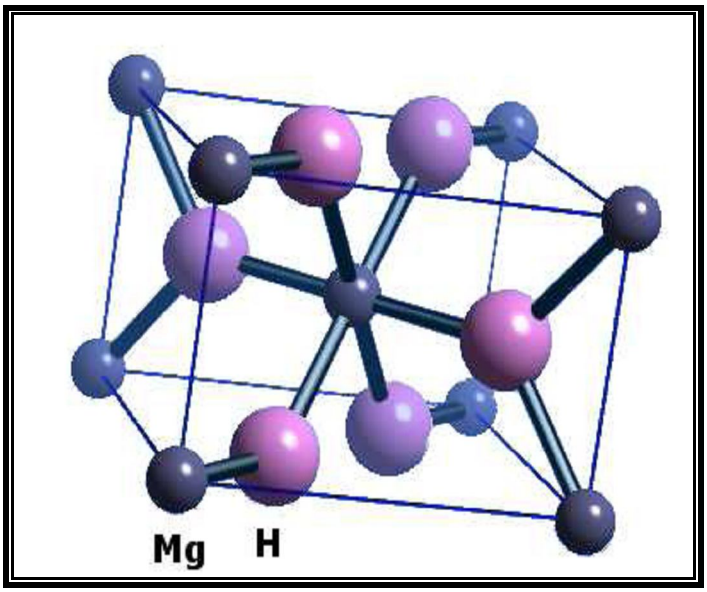

Fig. 2.4: Structure of MgH_2

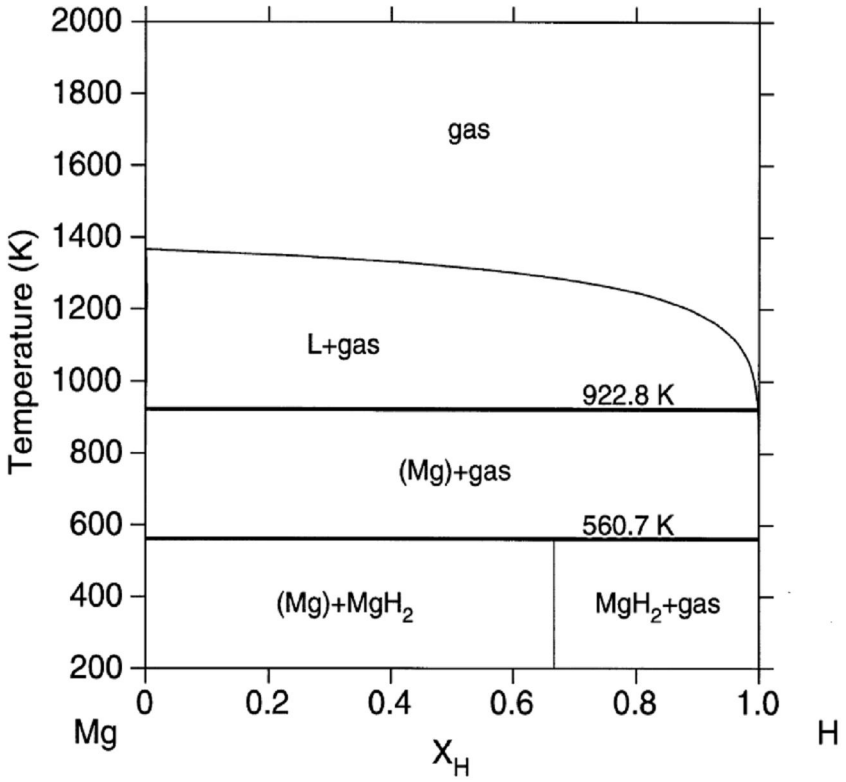

Fig. 2.5: Mg–H phase diagram at 1 bar

Fig. 2.5 shows the phase diagram of the Mg−MgH_2 system at 1 bar [22]. It can be seen that MgH_2 transforms to (Mg + Gas) at the dissociation temperature of 561 K. The melting point of Mg is 923 K. There is an influence of the gas pressure on the hydrogen solubility in solid and liquid Magnesium. The Mg based metal hydride is a promising use into many stationary and mobile applications, because of high hydrogen storage capacity. For this, selection of proper method to developed Mg hydride is the most important to suit the practical requirements. A few papers dealing with these tasks are presented here, which are available in literature.

Vigeholm et al (1980) investigated the reaction of hydrogen with commercially pure Magnesium powder (above 99.7%) in the temperature range 250–400 °C [23]. Hydrogen was readily absorbed above the dissociation pressure. During the initial exposure the Magnesium powder absorbed hydrogen slowly below 400 °C, but during the second exposure the sorption was fast from about 250 °C. It was nearly completed, when 400 °C was reached after 10 min. No change in the sorption rate was

observed with further cycling. In most experiments the resultant hydride was close to stoichiometric MgH_2. Desorption was found to be slower and to require higher temperatures than sorption, but was still practicable.

Ivanov et al (1987) studied Mg based systems such as Mg–Fe, Mg–Co, Mg–Nb and Mg–Ti, which cannot be prepared by conventional techniques. It can be fabricated by mechanical alloying, in addition to any other pairs or more complex mixtures of metals and non–metals [24]. They pointed out that intimate contact of metals can be achieved in high energetic ball mills. This contact played an important role in hydriding and dehydriding processes. They used two groups of catalytic additives. The first group was "hydrogen pumps" such as CeH_x. In the second group the added metal did not form any hydride in the conditions under study, but was known as an $H_2 \rightarrow$ H---H reaction catalyst (Cobalt, Nickel and probably Iron).

Klose and Stuke (1995) studied the influence of the solid in the Mg hydride system [25]. The amount of hydrogen absorbed by the solid in hydride system was experimentally estimated in dependence on the temperature, pressure and the stress-strains state of the solid. The existing hysteresis can be explained by the stress-strain state of the solid. A model was developed based on the conditions for chemical equilibrium that can qualitatively describe between hydrogen absorption and desorption. The assumptions made for estimating the stress-strain state of the solid imply some disagreements between the experimental and calculated results.

Fernandez and Sanchez (2002) studied the kinetics of hydrogen absorption and desorption by Magnesium by a volumetric technique [26]. Experimental data had been analysed in order to find the rate determining step for both the absorption and desorption processes. It was shown that a nucleation and growth mechanism, with exponent values n = 2 for desorption and n = 0.5 to n = l for absorption provides suitable equations in order to fit the experimental data. According to his claimed, the rate determining step in desorption of hydrogen by Magnesium, and probably also in the absorption process, seemed to be the hydrogen diffusion through the β–phase. An activation energy for such a diffusion process of 100 ± 10 kJ mol^{-1} H had been obtained from the desorption data.

Chen et al (2003) studied catalytic effect of multi–walled nano–tube (MWNT) on Mg composites by ball–milling under the hydrogen atmosphere [27]. It was found that under 2.0 MPa hydrogen pressure, the maximum hydrogen storage capacities of Mg–5 wt% MWNT was 5.34, 5.89 and 6.08 wt% at 373, 473 and 553 K respectively; but only 2.11, 2.68 and 2.75 wt% for Mg–20 wt% MWNT. Compared with other hydrogen storage composite materials, the Mg–5 wt% MWNT not only kept the maximum hydrogen storage capacities, but also had good hydrogen absorption/desorption rates. It absorbed 4.27, 4.86 wt% (80% maximum hydrogen storage capacity) within 15 and 1 min at 373 and 553 K under 2.0 MPa, while it desorbed 3.62 wt% within 30 min at 473 K. They claimed that the carbon component (the broken MWNT) in the composite might play an important role in the hydrogen uptake and release.

Hu et al (2003) investigated a Mg–30 wt% $TiMn_{1.5}$ hydrogen storage composite by mechanical milling of a mixture of Magnesium powder and amorphous $TiMn_{1.5}$ powder [28]. The hydrogen capacity was over 2.7 wt% at 373 K, and one absorption/desorption hydrogen cycle can be finished in 20 min at 523–573 K. Interestingly, the desorption temperature begins at about 500 K, decreasing about 40 K in contrast to that of the milled pure MgH_2.

Liang (2004) investigated the thermal stability and hydrogen storage properties of Mg–based alloys by mechanical alloying Mg with some transition and non–transition elements [29]. It was found that mechanical alloying results in a supersaturated solid solution of some elements in the Mg phase. Thermal annealing and/or hydrogenation cause irreversible decomposition of supersaturated solid solution leading to a composite of Mg or MgH_2 with other phase(s) depending on the composition and contents. Therefore, the plateau pressure or thermodynamic properties of hydrogen absorption/desorption of the supersaturated solid solution were no different from that of the Mg composite. While in some equilibrium systems, the formation of Mg solid solution was reversible upon hydrogenation/dehydrogenation. The plateau pressure of the hydrogenation/dehydrogenation was increased due to the interaction of the alloying elements with the Mg lattice in the solid solution. The Mg–Li system was an exception, because of the formation of stable LiH upon

hydrogenation of Mg (Li) solid solution. No interaction took place between Mg or MgH_2 with LiH. Therefore, no destabilization of MgH_2 was observed.

Kyoi et al (2004) investigated a Magnesium based Titanium doped hydride in a high–pressure anvil cell by reacting a mixture of MgH_2 and $TiH_{1.9}$ at 8 GPa and 873 K [30]. The metal structure had a Ca_7Ge type structure (a = 9.532(2) Å, space group Fm–3m (no. 225), Z = 4, V = 866.06 $Å^3$). The new hydride, Mg_7TiH_x exhibited 5.5 mass% ($x \approx 12.7$) and decomposed into Mg and $TiH_{1.9}$ upon releasing 4.7 mass% of hydrogen around 605 K.

Wagemans et al (2005) investigated the effect of crystal grain size on the thermodynamic stability of Magnesium and Magnesium hydride, using ab–initio Hartree–Fock and density functional theory calculations [31]. As expected, both Magnesium and Magnesium hydride became less stable with decreasing cluster size, notably for clusters smaller than 20 Magnesium atoms. However, Magnesium hydride destabilized more strongly than Magnesium. As a result, the hydrogen desorption energy decreased significantly, when the crystal grain size became smaller than ~ 1.3 nm. For instance, an MgH_2 crystallite size was 0.9 nm corresponds to a desorption temperature of only 200 °C.

Ming Au (2005) investigated nanostructured composite materials Mg–Ni, Mg–Ni–La, Mg–Ni–Ce and Mg–$LaNi_5$ using the mechanical alloying process [32]. The results show that amorphous/nanostructured composite material $Mg_{50wt\%}$–$Ni_{50wt\%}$ absorbed 5.9 wt% within 5 min and desorbed 5.1 wt% hydrogen within 15 min at 250 °C, respectively. He claimed that mechanical alloying that reduced particle size and introduces mechanical stress accelerates the hydrogenation kinetics of the Magnesium based materials even at low temperature. But, to release the absorbed hydrogen from the mechanical alloyed materials, a high temperature was still required. It was believed that the dehydriding temperature was largely controlled by the thermodynamic stability of Magnesium hydride. It was found that doping Mg–Ni nano/amorphous composite materials with Lanthanum, Cerium and $LaNi_5$ alloy reduce the hydriding and dehydriding temperatures. The composite material $Mg_{80wt\%}$–$(LaNi_5)_{20wt\%}$ absorbed 1.96% hydrogen and released 1.75% hydrogen at 25 °C, which suggested the formation of unstable hydrides. Although the stability of MgH_2 cannot

be easily reduced by ball milling alone, the results suggested the thermodynamic behavior of Mg–Ni nano/amorphous composite materials can be alternated by additives such as La, $LaNi_5$ or other effective elements.

Spassov et al (2005) investigated nanocrystalline $Mg_{87}Ni_3Al_3M_7$ (M = Ti, Mn, Mm; Mm= Ce, La–rich misch metal) hydrides by reactive mechanical milling (RMM) in hydrogen atmosphere [33]. The influence of the alloying elements (Ti, Mn, Mm) on the amount of the hydrides formed during RMM as well as on the temperature and enthalpy of hydrogen desorption was determined. The amount of hydride formed during RMM was found to be almost the same in the three alloys ~ 3.5 wt%. The Ti containing alloy revealed the lowest temperature of hydrogen desorption (~ 210 °C) and the hydride in the alloy with Mn decomposed at the highest temperature (~ 240 °C) among the three alloys studied. The enthalpy of H–desorption was highest for the sample alloyed with Mm (Ce, La), 70–72 kJ/mol; the Ti and Mn containing magnesium alloys had enthalpies 56–60 kJ/mol of hydrogen of hydride decomposition,. The alloys studied reveal higher equilibrium pressures of hydrogen absorption compared to nano–crystalline Magnesium, indicating some thermodynamic destabilization of the hydride as a result of the alloying. The hydrogen absorption in the Ti containing alloy was substantially faster than in the alloys with Mn and Mm.

Yao et al (2006) investigated the recent results of design and development of Magnesium based nano–composites demonstrating the catalytic effects of carbon nano-tubes and transition metals on hydrogen adsorption in these materials [34]. The results were promising for the application of Magnesium materials for hydrogen storage, with significantly reduced absorption temperatures and enhanced absorption/desorption kinetics. High level density functional theory calculations supported the analysis of the hydrogenation mechanisms by revealing the detailed atomic and molecular interactions that under the catalytic roles of incorporated Carbon and Titanium. It was providing clear guidance for further design and development of such materials with better hydrogen storage properties.

Wang et al (2006) studied Mg–Ce alloy by induction melting under vacuum, hydrided firstly and then Mg–Ce/Ni composite was obtained by mechanical milling, Mg–Ce hydrides under Ar for 50 h with addition of nano–sized Ni powder [35]. XRD results showed $CeMg_{12}$ formed in melted alloy. $CeMg_{12}$ disappeared and $CeH_{2.53}$ emerged during subsequent hydriding. Compared with Mg and Mg/Ni, Mg–Ce/Ni composite showed significant hydriding/dehydriding performance without any prior activation. The enthalpy of hydride formation for Mg–10.9 wt% Ce/10 wt% Ni composite was − 70.58 kJ mol^{-1} H_2. Improved hydrogen storage properties were attributed to the catalytic effect of addition of nano–sized Ni particles and existence of $CeH_{2.53}$, as well as the grain refinement, defects, etc. in the material introduced by ball milling process.

Hanada et al (2006) examined a catalytic effect of Niobium Oxide (Nb_2O_5) on the hydrogen storage properties of MgH_2 prepared by mechanical ball milling method [36]. The MgH_2 composite doped with 1 mol% Nb_2O_5 by ball milling for 20 h desorbed hydrogen up to 6 mass% in the temperature range from 200 to 250 °C at the heating rate of 5 °C/min under a purified Helium flow. After dehydrogenation at 200 °C, the product showed remarkable hydrogen absorption kinetics. A large amount of gaseous hydrogen up to 4.5 mass% was absorbed even at room temperature under 1 MPa hydrogen pressure within 15 s and finally its capacity reached up to 5 mass%. Furthermore, the valence state of Nb_2O_5 doped in MgH_2 was examined by X–ray absorption near edge structure (XANES) measurement. This suggested that the Nb compound, in which the valence state of Nb atom is less than +5, acts as a catalyst for the hydrogen absorbing/desorbing kinetics.

Ouyang et al (2007) studied effect of the rare earth and misch metal as a catalyst in Mg and synthesized Mg–La, Mg–Nd and Mg–misch metal systems by induction melting [37]. The alloys had good hydrogen storage properties and could absorb hydrogen at room temperature with rapid hydriding and dehydriding kinetics. The maximum hydrogen absorption content of Mg_3La, Mg_3Mm and Mg_3Nd alloys were 2.89, 2.58 and 1.95 wt%, respectively. Hydrogen absorption kinetic curves measured at room temperature could be well fitted by the Avrami–Erofeev equation.

Liu and Lei (2007) investigated the cyclic hydrogen storage properties of nano-crystalline composite of Mg–3Ni–2MnO_2 (wt %) by mechanical milling with Nickel nano–powders under hydrogen pressure [38]. The results showed that the composite had excellent hydrogen storage properties. Its maximum hydrogen capacity was about 6.5 wt%. The hydrogen absorption time was 50 s in which 6.37 wt% of hydrogen had been absorbed at 200 °C. The hydrogen desorption time was 310 s, in which the same amount of hydrogen had been discharged in the temperature range from 285 to 310 °C under hydrogen pressure of 0.1 MPa. The composite also had a better cyclic hydrogen storage property. After 60 times of cycling, the hydrogen capacity decreased less than 0.1 wt%. However, the hydrogen absorption time and desorption time were increased with the cyclic numbers. The reasons for these may be that the MgO, formed during the cycling process, impeded contact of the catalyst with the MgH_2.

Choi et al (2008) investigated the hydrogen release/uptake properties of the Mg–Ti–H system [39]. Samples were prepared from the mixtures of MgH_2 and TiH_2 in molar ratios of 7:1 and 4:1 using a high–energy–high–pressure (HEHP) mechanical ball–milling method under 13.8 MPa hydrogen pressure. Thermo–gravimetric analysis showed that a relatively large amount of hydrogen (5.91 and 4.82 wt%, respectively, for the above two samples) was released between 126 °C and 313 °C, while temperature was increased at a heating rate of 5 °C min^{-1} under an argon flow. The onset dehydrogenation temperature of these mixtures, which is 126 °C, was much lower than that of MgH_2 alone, which was 381 °C. The activation energy of dehydrogenation was 71 kJ mol^{-1}, which was much smaller than that of as–received MgH_2 (153 kJ mol^{-1}) or as–milled MgH_2 (96 kJ mol^{-1}). Furthermore, the hydrogen capacity and the dehydrogenation temperature remained largely unchanged over five dehydrogenation and rehydrogenation cycles.

Lucaci et al (2009) investigated enhanced hydrogen storage capacity of the Magnesium alloys by adding some elements such as Ti, Fe and Ni, by mechanical alloying [40]. The $Mg_{76}Ti_{12}Fe_{12-x}Ni_x$ (x = 4, 8) alloys were prepared by mechanical alloying for 10 h, 20 h and 60 h in petroleum ether medium, followed by a subsequent thermal treatment at 450 °C for 3 h, in Argon atmosphere. Increasing of milling time

generated single–phase materials having enhanced homogeneity. The $Mg_{76}Ti_{12}Fe_{12-x}Ni_x$ (x = 4) material had a hydrogen storage capacity of 5.33 wt% hydrogen, which was totally reversible. These materials can be used for the high temperature hydrogen storage applications.

Shelyapina et al (2010) studied mixing of Mg or MgH_2 with small amount of transition metals or their oxides and showed remarkably improvement of the hydrogen kinetics [41]. Recently a series of new hydrides Mg_7TiH_x, $Mg_{6.5}NbH_x$ and Mg_6VH_x of Ca_7Ge type structure had been synthesized. The hydrogen desorption properties had been found to be better than for pure MgH_2. Here, they report on the results of the electronic structure of these new hydrides within the framework of the full–potential, self–consistent linearized augmented plane–wave method. They used these results, along with calculations of the heat of formation and relative stability to discuss the bonding of these materials and their hydrogen–storage properties.

Banerjee et al (2010) investigated the interaction of hydrogen with pure and Ti doped Mg clusters using density functional theory [42]. For Mg_{55} cluster, the activation energy of hydrogenation was calculated to be 0.72 eV, which was 30% less than the bulk value of 1.04 eV. The interaction of hydrogen with Mg_{55} and $TiMg_{54}$ clusters gave the binding energy of 0.217 and 0.164 eV, respectively. Moreover, the activation energy calculated by the elastic band method reveals that the dissociation barrier of hydrogen was 0.72 and 0.58 eV for Mg_{55} and $TiMg_{54}$, respectively. Thus, they could show a significant reduction in the activation barrier (almost 40%) of hydrogen dissociation in small clusters than the bulk. This had been attributed to the combined effects of the finite size of Mg clusters and the catalytic influence of Ti substitution.

2.4.2 AB Type

The AB alloys store hydrogen at a low cost and exhibit plateau pressures of a few atmospheres at temperatures up to 100 °C. Most of the work done on AB compounds had been restricted to Fe–Ti, which had a CsCl type crystal structure. In Fe–Ti systems, Iron and Titanium were form two known stable intermetallic compounds [43]. Two hydrides; a monohydride with a tetragonal structure and a dihydride with a

cubic structure were formed. It was necessary to initially activate Fe–Ti, before it reacted at a practical rate with hydrogen. Reaction kinetics was considerably slower. Other disadvantages of the Fe–Ti–H system were pronounced hysteresis and the weight of the alloys. These problems can be eliminated to some extent by the substitution of various alloying elements such as Mn and Al for Fe. Manganese substitution reduced hysteresis and provides some resistance to poisoning, while Aluminum reduced the overall weight of the alloy. *Sasai et al* (1983) studied difficulty regarding activating Fe–Ti system [44]. The addition of Zirconium as a third element and Niobium as a fourth element in the concentration range 0.5–5 at% improved the easy activation of Fe–Ti system. Thus, it was now possible to activate this alloy at a hydrogen pressure of 20–30 bar and room temperature. Another, AB type alloy system was Zr–Ni, which had 1.85 mass% of hydrogen storage capacity at desorption temperature 565 K.

2.4.3 A_2B Type

The best example of A_2B type metal hydride was Mg_2Ni. At room temperature, the nano–crystalline Mg_2Ni alloy absorbed hydrogen, but almost did not desorb it. At temperature above 523 K, the kinetic of the absorption–desorption process improved considerably and for nano–crystalline Mg_2Ni alloy the reaction with hydrogen was reversible. The hydrogen content in this material at 573 K was 3.25 wt% [45, 46]. During the hydrogenation, Mg_2Ni phase was transformed into the hydride Mg_2NiH_x phase. It was important to note that the hydride Mg_2NiH_x phase transformed from a high temperature cubic structure to a low temperature monoclinic phase. When hydrogen was absorbed by Mg_2Ni beyond 0.3 H per formula unit, the systems undergo a structural rearrangement to the stoichiometric complex Mg_2NiH_x hydride, with an accompanying 32% increase in volume. The electrochemical properties of the alloy were improved after substitution of some amounts of Magnesium by Mn, Co, Ce, and Ti [47].

Janot et al (2004) investigated the sorption kinetics of Mg_2Ni alloys using two different surface treatments [48]. One consists of the preparation of tailor–made Mg_2Ni/C composites by ball–milling with previously ground carbons. The strong reducing character of carbon, allowing for the reduction of NiO initially present at the

alloy surface, lead to the partial removal of the oxide layer. There was resulting Ni particles act as catalysts during the absorption process. The second surface treatment was deal with the deposition of Pd particles on the alloy surface using the polyol process. The catalytic effect of Pd was responsible for an important enhancement of the absorption kinetic. Moreover, Pd particles probably acted as hydrogen pumps, during the desorption process, leading to a faster hydrogen release. By combining both techniques, desorption rated as high as 2.7 wt% in 60 min and 2.9 wt% in 30 min were obtained at 150 and 200 °C, respectively.

2.4.4 AB_2 Type

The research on AB_2 (A=Zr, Ti, and B=V, Cr, Mn, Fe, Co, Mo and Al) type Laves phase hydrogen storage alloys started early in the 1960. In ZrB_2 compounds for B=V, Cr and Mn the alloys could absorb and desorbed large quantities of hydrogen (Shaltiel 1978) [49]. In AB_2 Laves phase alloys, as the atomic radius of element A is much bigger than that of B (optimum ratio $r_A/r_B = 1.225$), the atoms were arranged in very compact layered lattice structure with 17 tetrahedral interstitial cavities. In which, there were potential sites for storing hydrogen atoms. The AB_2 compounds had a high storage capacity, showed good resistance to impurities and exhibit low hysteresis. The best sorption characteristics had been observed for ZrV_2, $ZrCr_2$, and $ZrMn_2$ with 6 hydrogen atoms per formula unit. But they suffered from excessive stability of their hydrides, manifested by high heat of formation and very low plateau pressures.

2.4.5 AB_5 Type

In the late 1960s *Van Vugt et al.* at the Philips Eindhoven Lab investigated the permanent magnet properties of AB_5 intermetallics [50]. By accident, they discovered the exceptional hydriding properties of these materials, especially $LaNi_5$. This particular intermetallic compound could readily and reversibly absorb 6 hydrogen atoms per formula unit at ambient temperature under an equilibrium pressure of about 2 bar. These remarkable properties made this alloy a very good candidate as a potential hydrogen storage material [51].

Today the hydride forming materials based on the AB_5 intermetallics were the most versatile and commercial important family of reversible hydriding alloys. In these alloys, the A elements were usually taken from rare earth elements of the lanthanide group with atom number from 57 to 71. In addition, Calcium was also used as an A element. As B element, Nickel was the most used element, often in combination with other transition metals. The ratio between the A and B elements were restricted to values close to 1:5 [52]. AB_5 intermetallic compounds were the most used materials for negative electrodes in nickel metal hydride batteries. Already in the 1970s, it was reported that $LaNi_5$ could be utilized as a negative electrode material in nickel metal hydride batteries (NiMH) [53]. However, in such applications $LaNi_5$ exhibited too high equilibrium pressure and too short cycle life time to be of practical interest for commercial batteries. The short cycle life time, (the dramatic capacity loss during cycling) was probably due to oxidation of the Lanthanum to $La(OH)_3$ and formation of Nickel particles. This was compensated by modification of the alloy by substitution of Nickel by other transition metals. The solid solubility of the B–type substitution atoms depends on the substitution element. For example, the solid solution $LaNi_{5-x}M_x$ was total for M = Co, Pt or Cu, but partial for Si ($x \leq 0.6$), Fe ($x \leq 1.2$), Al ($x \leq 1.3$) or Mn ($x \leq 2.2$). A partial replacement of Nickel by Cobalt had a particularly positive influence on the long–term cyclic stability of the AB_5 materials.

On the other side, the Lanthanum atoms in $LaNi_5$ can be substituted by Lanthanide elements in the whole concentration range leading to complete solid solution for the rare earths. The A–type atoms (Lanthanum) were frequently replaced with a Mischmetal (Mm) of rare earths [54]. This was initially done due to economic reasons, but it had later been shown that the composition of the Mischmetal was important for the cycle lifetime. The optimal composition for electrode purposes had been found $MmNi_{3.55}Mn_{0.4}Al_{0.3}Co_{0.75}$ composition [55].

2.5 Estimation of the Fractional Hydrogen into Metal

The metal hydride is the safest physical hydrogen storage media. It works simply. Hydrogen is absorbed under certain temperature and pressure, and thereafter it released under another set of specific conditions. The number of hydrogen molecules absorbed or desorbed is the important parameter of the metal hydride especially for

mobile applications and known as a hydrogen storage capacity. It is estimated using following way:

2.5.1 Using Ideal Gas Equation

For computing the efficiency of a hydriding alloy, hydrogen absorption measurement is carried out on the principle of pressure reduction method in a hydriding reactor [56]. The hydrogen concentration in the form of mass % is calculated from the pressure drop during the absorption reaction in a calibrated volume space at constant hydriding temperature using the ideal gas law, as:

The number of moles of hydrogen gas with isolation of reactor can be written as:

$$n = \frac{\Delta P \times V}{R \times T} \qquad \text{---------- (2.12)}$$

Where, ΔP is the pressure drop, V is the volume of the reactor chamber, R is the gas constant and T is the absolute temperature.

Therefore, the mass of H_2 gas absorbed in metal alloy/composition is nothing, but multiplication of molecular weight of hydrogen and number of moles of absorbed hydrogen (n).

$$\therefore \text{ Mass \% of hydrogen absorbed in metal hydride} = \frac{m}{m+M} \times 100\% \qquad \text{---------- (2.13)}$$

Where, M is the mass of sample.

Similarly, an expression can be developed for computing the mass percent of hydrogen desorbed during the dehydriding reaction.

2.5.2 Using Real Gas Equations

However, the ideal gas equation of state can be only derived from kinetic theory, if assumptions of no attractive forces between molecules are made and volume of gas molecules is neglected [57]. These assumptions are strictly valid only under the following parametric conditions:

$$\frac{PV}{RT} \to 1 \quad and \; P \to 0 \qquad \text{---------- (2.14)}$$

During the hydriding process, the above conditions are usually never satisfied, as the hydriding reaction is conducted under high steady state reactor pressure, at elevated temperature. This is especially true for work on "high enthalpy–of–hydriding" alloy systems. Such as those based on the metal Magnesium, for which hydriding temperature greater than 300°C are typically required at pressure higher than 30 atm. Under these conditions, significant departure from ideality can occur, leading to significant error in estimates of the absorption/desorption capacities. Further, for the purpose of chemical reaction engineering and kinetics modeling, the accuracy requirement is typically of the order of 0.1% in the basic reaction time – reactant mass data. Hence, it is imperative that the magnitude of the deviations expected in typical hydriding reactions are systematically estimated using more appropriate equations of state for hydrogen.

In the present discussion, the deviations due to departure from ideality using three different equations of state for real gases have computed. These equations are the Van–der–Waal, Redlich–Kwong and Redlich–Kwong–Soave equations and are detailed below [58]:

2.5.2.1 The Van–der–Waal Equation of State

The Van–der–Waal's equation of state can be written as:

$$\left(P + \frac{a}{\bar{v}^2}\right)(\bar{v} - b) = RT \qquad \text{---------- (2.15)}$$

Where; a and b are the Van–der–Waal's constants, $\bar{v}$ is the molar specific volume and P is the pressure.

2.5.2.2 The Redlich–Kwong Equation of State

Redlich and Kwong presented a two–constant equation of state and that is more accurate than the Van–der–Waals equation. This equation is represented as:

$$P = \frac{RT}{(\bar{v} - b_1)} - \frac{a_1}{\bar{v}(\bar{v} + b_1)T^{0.5}} \qquad \text{---------- (2.16)}$$

Where; a_1 and b_1 are the Redlich and Kwong defined constants.

2.5.2.3 The Redlich–Kwong–Soave Equation of State

A further improvement over the Redlich–Kwong equation of state called the Redlich–Kwong–Soave equation is a three–constant equation, and is represented as:

$$P = \frac{RT}{(\bar{v} - b_1)} - \frac{a_1}{\bar{v}(\bar{v} + b_1)T^{0.5}} \left\{ 1 + m \left[1 - \left(\frac{T}{T_c} \right)^{0.5} \right] \right\}^2$$

And, $$m = 0.48 + 1.574\omega - 0.176\omega^2 \qquad \text{---------- (2.17)}$$

Where; ω is the acentric factor (a constant for a given gas, for example it is –0.215 for Hydrogen).

Using the ternary/quaternary Mg based alloy systems as the model "large hydriding enthalpy" alloys. The significant overestimates of uptake and desorption of hydrogen can be made, if the reaction kinetics data is generated using only the ideal gas law model. These computational studies are presented in the chapter 4. Since the observed deviations are not suitable for undertaking chemical reaction engineering work for large scale reactor design as well as for kinetics modelling. It is difficult to rationalize use of the ideal gas assumption for undertaking studies on "large hydriding enthalpy" hydrogen storage alloys.

2.6 Reaction Kinetics of the Solid State Hydrogen Storage

Equations describing the transport of hydrogen for each of the steps, describing in section 2.2, are well known. Linking the sequence of individual equations can yield the reaction rate at each given point of time. Recently, study on a combined model based on sequence of partial steps to describe the development of hydride on spherical powder particles, in which the hydride phase is growing from the sample surface towards the center. The application of the coupled equations method to the overall kinetic curve of a real case is somewhat complicated by the following reasons [59]:

(i) For un–activated samples, the initial stage of the hydriding reaction is controlled by the transport of hydrogen through the surface passivation layer (SPL). The kinetics of this initial stage is different in nature from the succeeding processes performed by the formation of the hydride layer.

(ii) Activated powder samples are usually free of the SPL initial effects. However, they may suffer from other problems. For example, temperature increases during the hydriding process, the effect of the time delay of the starting point of each powder particle, etc.

(iii) Cracking of the parent metal/alloy (especially in the case of inter–metallic) or of the product hydride layer (in the case of pure metals) may affect the kinetics.

(iv) The final parts of the reaction, where the symmetry is lost may also change the kinetics.

(v) The reaction rate depends on the sample's geometry and dimensions.

In the present study, a slightly different approach is assumed. Instead of the whole reaction kinetics, there are concentrated upon the net hydrogen absorption during a specific part of the reaction. It is assumed to determine the rate laws for governing the hydriding process. A part which is less affected by the aspects considered above. Here, first describe simple first order kinetics model. The relations between the rate of hydrogen absorption during the steady state stage and the system

parameters (namely, the hydrogen pressure, the critical concentrations of hydrogen in the hydride, and the rate constants associated with the individual steps), known as spherical shrinking core model is also studied. Finally, kinetics effect on a nucleation and growth of hydride phase of the metallic surface, known as a Johnson–Mehl–Avrami model is presented [60].

2.6.1 First Order Model

The experimental data of the synthesized alloy is first modelled using a first–order lumped exponential response model of the form [61]:

$$M_c\% = \alpha_c\left[1 - e^{-\beta_c t}\right] \text{ (For charging kinetics)} \quad \text{---------- (2.18)}$$

$$M_d\% = \alpha_d e^{-\beta_d t} \text{ (For discharging kinetics)} \quad \text{---------- (2.19)}$$

Where, M_c % & M_d % are the mass percent hydrogen during absorption and desorption, respectively; α_c & α_d are the charging and discharging reaction constants, respectively; $1/\beta_c$ & $1/\beta_d$ are the charging and discharging time constants, respectively and t is the time.

The experimental constants in the above two equations are determined using linear regression and predictions of the estimated models are compared with experimental data (chapter 4). In the next section, the reaction kinetics by the more sophisticated shrinking core model has explained.

2.6.2 Shrinking Core Model (SCM)

This model is used to describe situations in which solid particles are being consumed either by dissolution or reaction and, as a result, the amount of the material being consumed is ‘shrinking’ [62, 63] (see Fig. 2.6). This model applies for fitting the hydrogen absorption data. Hydriding reactions in which a hydride layer is formed on top of the parent metal, moving continuously into the sample’s center, are referred to as to as ‘the contracting envelope’ or ‘the shrinking core’ mechanism. Typically, after

an initial acceleration stage a steady state process is maintained during, which the rate of advance of the hydride layer is constant.

For this purpose, we consider the hydriding reaction (see Fig. 2.7):

$$H_{2(g)} + \beta_{(s)} \rightarrow \beta H_{2(s)} \qquad \text{---------- (2.20)}$$

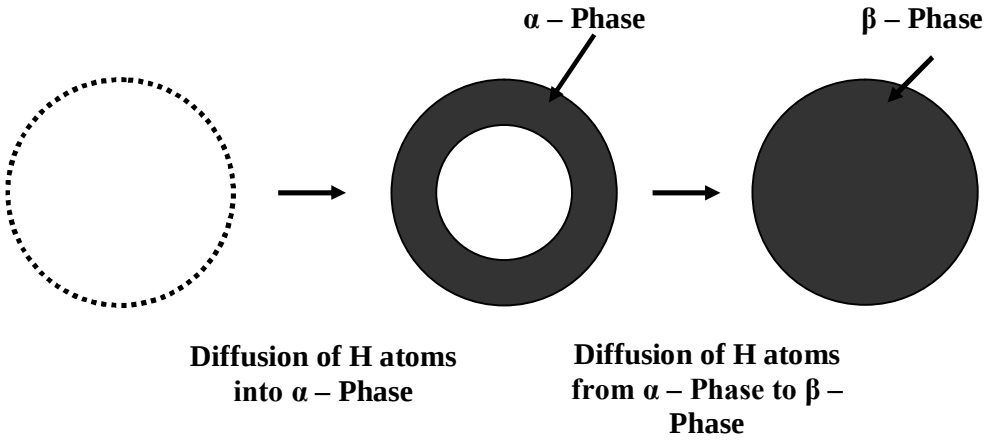

Fig. 2.6: Schematic diagram of shrinking core model

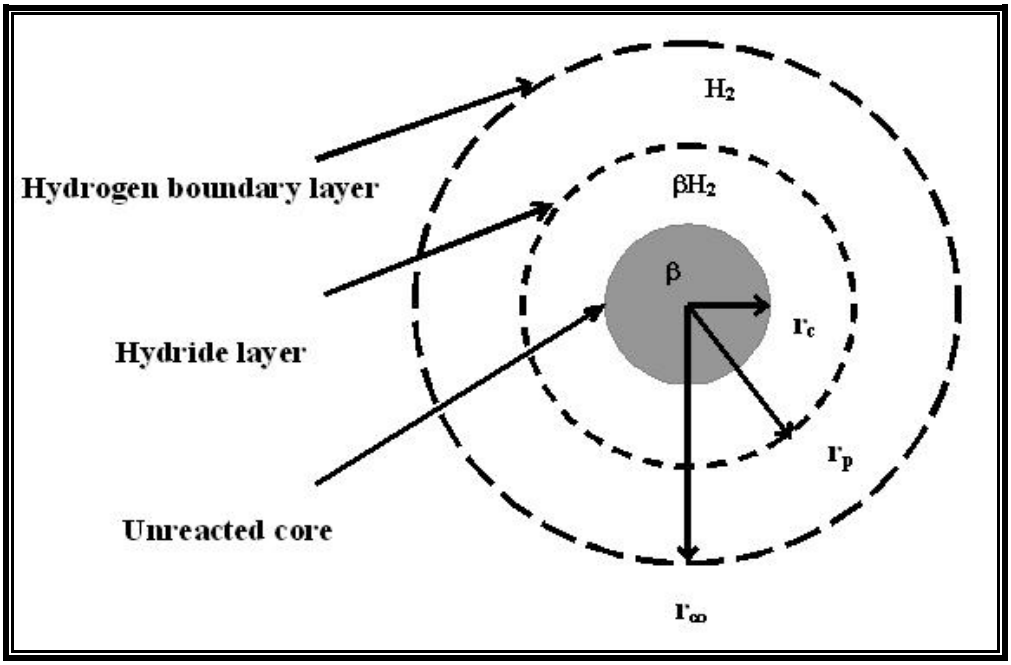

Fig. 2.7: Schematic diagram showing the three–core spherical shell of the three phases involved in hydriding reaction

The rate at which an individual spherical particle reacts is determined by mass transfer of reactant through the boundary, diffusion through hydride layer, and finally chemical reaction at the interface. It can be shown that for a fixed gas phase (H_2) concentration, the converted mass fraction of β at time t, X_β^t is related to three dimensionless parameters t^*, Φ_1 & Φ_2 as below:

$$t^* = \left[1-\left(1-X_\beta^t\right)^{1/3}\right]\left\{1+\frac{\phi_1\phi_2}{3}\left[\left(1-X_\beta^t\right)^{2/3}+\left(1-X_\beta^t\right)^{1/3}+1\right]+\frac{\phi_2}{6}\left[\left(1-X_\beta^t\right)^{1/3}+1-2\left(1-X_\beta^t\right)^{2/3}\right]\right\}$$

---------- (2.21)

Where; t^* is the dimensionless time; Φ_1 is the ratio of the external diffusion resistance and diffusion resistance in product layer; and Φ_2 is the ratio of the diffusion resistance in product layer and reaction resistance at β/γ interface.

Further, if chemical reaction at $\beta/\beta H_2$ interface purely controls the reaction, then $\phi_2 \equiv 0$ and we can write Eq. (2.21) as:

$$t = \frac{\rho_\beta r_p}{M_\beta k_r (c_\alpha)_\infty}\left[1-\left(1-X_\beta\right)^{1/3}\right]$$

---------- (2.22)

Where; ρ_β is the density of species β, r_p is mean radius of spherical powdered phase of reactant, M_β is molecular weight of species β, k_r is reaction rate constant at $\beta/\beta H_2$ interface and $(C_\alpha)_\infty$ is far-zone concentration of α in reactor.

Similarly, if diffusion through product phase is purely controlling, $\phi_1 \equiv 0$, then Eq. (2.21) can write as:

$$t = \left(\frac{\rho_\beta r_p^2}{6D_p M_\beta (c_\alpha)_\infty}\right)\left[1-3\left(1-X_\beta^t\right)^{2/3}+2\left(1-X_\beta^t\right)\right]$$

---------- (2.23)

Where; D_P is the diffusion coefficient through species βH_2 of α.

Equations (2.22) and (2.23) are both "$\hat{Y} = A\hat{X}$" type linear equations. Based on a constrained (zero intercept) linear regression model, the predictions of Eqns. (2.22) and (2.23) are compared with the experimental results for the ternary/quaternary Mg based alloys system (chapter 4).

2.6.3 Johnson–Mehl–Avrami Model (JMA Model)

When experimental kinetic data is fitted with a rate equation, both hydride nucleation and growth or diffusion processes are assumed to be rate limiting steps. Nucleation and growth kinetics is usually explained by a Johnson–Mehl–Avrami (JMA) rate equation [64, 65]. The JMA equation has the following form,

$$\alpha = 1 - e^{(-kt)^n} \qquad \text{---------- (2.24)}$$

Or, another way,

$$\ln\left[-\ln(1-\alpha)\right] = n\ln t + n\ln k \qquad \text{---------- (2.25)}$$

Where, α is the fraction reacted of hydrogen at time, t and rate constant, k. The exponent, n, referred as the Avrami exponent is an integer or non integer, the value of which is governed by the geometries associated with the rate–controlling process. The temperature dependency of the rate constant k is usually described by an Arrhenius relation [66],

$$k = Ae^{\left(-\frac{E_a}{RT}\right)} \qquad \text{---------- (2.26)}$$

Where, A is a pre-exponential factor, E_a is the apparent activation energy and R is the gas constant. The most interesting property of the JMA equation is that it explains the diffusion rate limiting step, when n is having values of 1 or less. For the Nucleation and growth rate limiting steps, Avrami exponent, n is having values of greater than 1. Hence, JMA model is often successfully invoked in dealing the kinetics of hydrogenation/dehydrogenation of metal hydrides. Even though the JMA

equation may provide a good fit, any conclusions about nucleation and growth being rate limiting in such a process should be considered with care.

2.7 Thermodynamic Properties (ΔH and ΔS)

2.7.1 The Pressure Composition Isotherm (PCI)

The absorption–desorption process of metal hydrides systems is represented by means of the pressure composition isotherm (PCI diagrams) [67 – 69]. A generic PCI curve is showed in Fig. 2.8. This curve describe the hydrogen dissociation pressure (absorption/desorption pressure, hydrogen equilibrium pressure or plateau pressure), P_{H2} as a function of hydrogen concentration. When initially increasing the hydrogen pressure at isothermal conditions the absorbed amount of hydrogen (H/M is the hydrogen to metal stoichiometric ratio) will increase only slightly. This corresponds to the formation of a solid solution of hydrogen and this is denoted the α–phase. At one specific pressure the hydriding reaction begins and the metal starts to absorb large quantities of hydrogen at constant pressure (plateau pressure). After, the metal has completely been transformed into metal hydride, the pressure increases again steeply. This hydride phase is known as β–phase. Increasing the hydrogen pressure further will now result in a substantial increase in the absorbed amount of hydrogen.

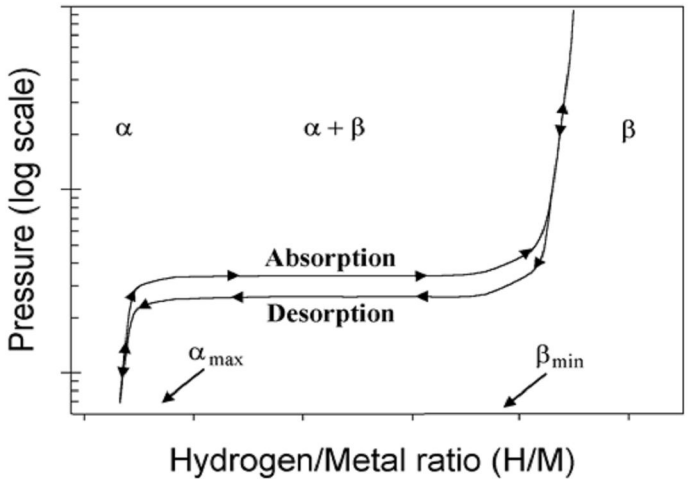

Fig. 2.8: PCI diagram of metal hydrides

This phenomenon may be explained from the Gibbs phase rule [70 – 72];

$$F = 2 - \pi + N \qquad \text{---------- (2.27)}$$

Where F is the degree of freedom, π is the number of phases and N is the number of chemical species. Thus, existence of one additional phase leads to the loss of a degree of freedom. The pressure at which this transformation takes place is referred to as the plateau pressure and in this region the α–phase and β–phase co–exist. When the stoichiometric hydrides have formed completely depleting the α–phase one additional degree of freedom is regained and the additional absorption of hydrogen will now require a large pressure increase. This corresponds to the solid solution of hydrogen in the β–phase. The plateau pressure gives valuable information about reversible storage capacity from the width of the plateau and the position of the plateau at a given temperature may give an idea of the stability of the hydride. Stable hydrides will require higher temperatures than less stable hydrides to reach a certain plateau pressure.

Fig. 2.8 also exhibits a hysteresis effect and a sloped plateau. Hysteresis effect is not desirable in practical applications as at the same temperature, hydrogen is released at a pressure slightly lower during desorption than absorption. Apart from hysteresis, another irreversibility that reduces the system efficiency is the sloped plateau. In actual systems all the hydrides possess sloped plateau, the magnitude of which varies greatly from material to material. Because of the plateau slope, the equilibrium pressure in the (α+β) increases with concentration during absorption and decreases with concentration during desorption. This reduces the usable hydrogen capacity, the heat and mass transfer rates also reduce with plateau slope, as a result the system performance is reduced. It is possible to reduce these irreversibilities by varying the alloy composition.

Two important thermodynamic parameters of metal hydride formation can be deduced from the plateau of the PCI diagram. These are the standard enthalpy of formation (ΔH) and standard Gibbs free energy of formation (ΔG). Neglecting the

small concentration increase during the α–phase, the metal hydride reaction for the α+β phase is given by,

$$M + \frac{y}{2} H_2 = MH_y \qquad \text{---------- (2.28)}$$

The Van't Hoff isochoric relation for the above reaction is given by [73, 74],

$$\frac{\partial(\ln K_P)}{\partial T} = \frac{\Delta H}{RT^2} \qquad \text{---------- (2.29)}$$

Where, K_P is the equilibrium constant of the hydriding reaction and T is the absolute temperature. Since in this case only hydrogen gas reacts with a solid (metal hydride), the equilibrium constant is given by,

$$K_P = P_{H_2}^{-y/2} \qquad \text{---------- (2.30)}$$

Substituting Eq. 2.30 into Eq. 2.29 and integrating,

$$\ln P_{H_2} = \left(\frac{-2}{y}\right)\left(\frac{\Delta H}{RT}\right) + C \qquad \text{---------- (2.31)}$$

Thus, from the plots of equilibrium pressure P_{H2} versus 1/T, standard heat of formation (slope of the line) and the constant of integration C (intercept of the line) can obtain. Then the Gibbs free energy (ΔG) and standard entropy of formation (ΔS) can be obtained by,

$$\Delta G = -RT \ln K_P = \frac{y}{2} RT \ln P_{H_2} \qquad \text{---------- (2.32)}$$

$$\Delta S = \frac{1}{T}(\Delta H - \Delta G) \qquad \text{---------- (2.33)}$$

2.7.2 Van't Hoff Relationship

The plateau pressure, P_{H2} is dependent on the temperature T and linked with the reaction enthalpy ΔH by the following Van't Hoff equation [75–78]:

$$\ln \frac{P_{H_2}}{P_0} = \frac{\Delta H}{RT} - \frac{\Delta S}{T} \qquad \text{---------- (2.34)}$$

The plot of the natural logarithm of (P_{H2}/P_0) against the inverse temperature yields the reaction enthalpy resulting from the slope of the Van't Hoff–line according to:

$$\Delta H = R \frac{\ln \frac{P_{H_2}}{P_{h_1}}}{\frac{1}{T_2} - \frac{1}{T_1}} \qquad \text{---------- (2.35)}$$

The Van't Hoff relations of different metal hydrides are shown in the Fig. 2.9 [79–81]. Certain pressure/temperature pairs of values are selected for defined hydrogen concentrations.

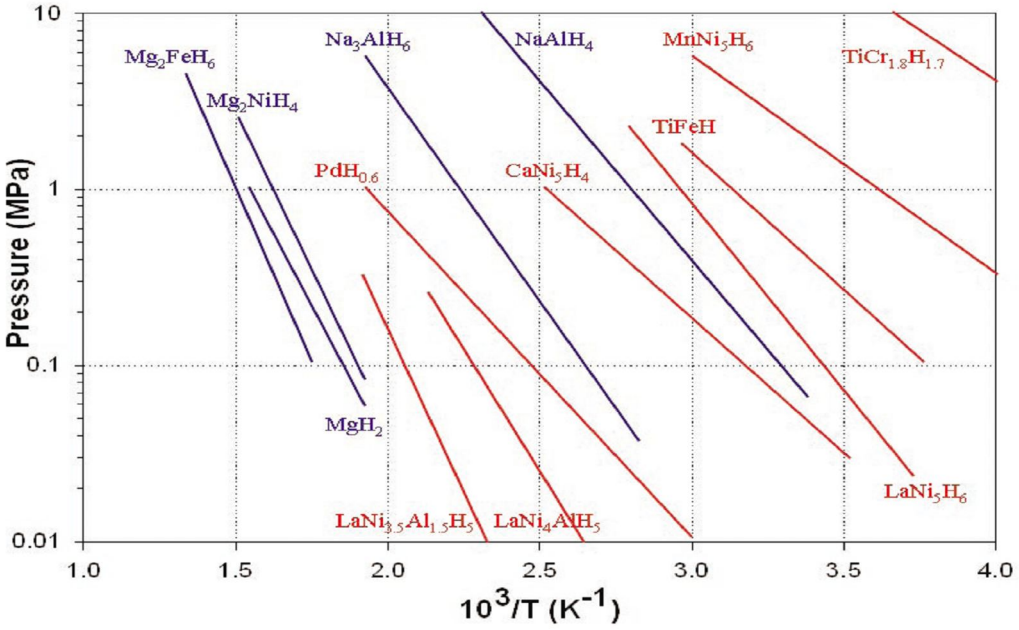

Fig. 2.9: The Van't Hoff relation of different metal hydrides

The slope can be calculated by the linear regression method as following:

$$Y = BX + A = \ln\left(\frac{P_{h_2}}{P_0}\right) = \left(\frac{\Delta H}{R}\right)\frac{1}{T} + \left(-\frac{\Delta S}{T}\right) \qquad \text{---------- (2.36)}$$

By comparing the coefficients, the reaction enthalpy ΔH and the reaction entropy ΔS can be determined.

REFERENCES

1. www.folk.uio.no.//ravi//activity//hydride
2. M. Sahlberg, Light Metal Hydride for Hydrogen Storage, *Ph. D. Dissertation* (2009) ACTA Universitatis, Upsaliensis, Uppsala.
3. M. Peruzzini and R. Poli, Recent Advanced in Hydride Chemistry, *Elsevier press*, Amsterdam–London–New York–Oxford–Paris–Shannon–Tokyo (2001) 531–545.
4. A. Borgschulte, R. J. Westerwaal, J. H. Rector, H. Schreuders, B. Dam and R. Griessen, *J. of Catalysis*, **239** (2006) 263–271.
5. C. S. Sunandana, "Nanomaterials for Hydrogen Storage", *Resonance* (2007) 31–36.
6. J. Purewal, Hydrogen Adsorption by Alkali Metal Graphite Intercalation Compounds, *Ph. D. Dissertation* (2010) California Institute of Technology, Pasadena, California.
7. A. Zuttel, *materialstoday*, **6** (2003) 24–33.
8. A. Zuttel, *Naturwissenschaften*, **91** (2004) 157–172.
9. A. Andreasen, Hydrogen Storage Materials with Focus on Main Group I–II Elements, *Ph. D. Dissertation* (2005) Risø National Laboratory, Denmark.
10. Kuo–Chih Chou, Qian Li, Qin Lin, Li–Jun Jiang and Kuang–Di Xu, *Int. J. of Hydrogen Energy*, **30** (2005) 301–309.
11. Q. Lia, K. Chou, Q. Lin, L. Jiang and F. Zhan, *Int. J. of Hydrogen Energy,* **29** (2004) 1383–1388.
12. B. Panella, Hydrogen Storage by Physisorption on Porous Materials, *Ph. D. Dissertation* (2006) Max–Planck–Institut fur Metallforschung, Stuttgart.
13. M. Martin, C. Gommel, C. Borkhart and E. Fromm, *J. of Alloys and Compounds*, **238** (1996) 193–201.
14. D. R. Lide (Ed.), Handbook of Chemistry and Physics, 78th Edition, *CRC Press LLC* (1997).
15. W. Grochala and P. P. Edwards, *Chem. Rev.*, **104** (2004) 1283–1315.
16. R. Checchetto, N. Bazzanella, A. Miotello and P. Mengucci, *J. of Alloys and Compounds*, **446–447** (2007) 58–62
17. H. Smithson, C. A. Marianetti, D. Morgan, A. Van der Ven, A. Predith and G. Ceder, *Phys. Rev. B,* **66** (2002) 144107–1.

18. T. Norikate, M. Aoki, S. Towata, Y. Seno, Y. Hirose, E. Nishibori, M. Takata and M. Sakata, *Appl. Phys. Letters,* **81** (2002) 2008–2010.
19. L. Schlapbach and J. P. Bueger, *J. Physique. Letters*, **43** (1982) 273–276.
20. K. C. Hoffman, J. J. Reilly, F. J. Salzano, C. H. Waide, R. H. Wiswall and W. E. Winsche, *Int. J. of Hydrogen Energy*, **1** (1976) 133–151.
21. www.webelements.com
22. K. Zeng, T. Klassen, W. Oelerich and R. Bormann, *Int. J. of Hydrogen Energy*, **24** (1999) 989–1004.
23. B. Vigeholm, J. Kjqller and B. Larsen, *J. of the Less Common Metals*, **74 (2)** (1980) 341–350.
24. E. Ivanov, I. Konstanchuk, A. Stepanov and V. Boldyrev, *J. of the Less Common Metals*, **131 (1–2)** (1987) 25–29.
25. W. Klose and V. Stuke, *Int. J. Hydrogen Energy*, **20 (4)** (1995) 309–316.
26. J. F. Fernandez and C. R. Sanchez, *J. of Alloys and Compounds*, **340 (1–2)** (2002) 189–198.
27. D. Chen, L. Chen, S. Liu, C. X. Ma, D. M. Chen and L. B. Wang, *J. of Alloys and Compounds*, xxx (2003) xxx–xxx.
28. Y. Q. Hu, H. F. Zhang, A. M. Wang, B. Z. Ding and Z. Q. Hu, *J. of Alloys and Compounds*, **354 (1–2)** (2003) 296–302.
29. G. Liang, *J. of Alloys and Compounds*, xxx (2004) xxx–xxx.
30. D. Kyoi, T. Sato, E. Rönnebro, N. Kitamura, A. Ueda, M. Ito, S. Katsuyama, S. Hara, D. Noréus and T. Sakai, *J. of Alloys and Compounds*, **372** (2004) 213–217.
31. R. W. P. Wagemans, J. H. van Lenthe, P. E. de Jongh, A. Jos van Dillen and K. P. de Jong, *J. AM. Chem. Soc.*, **127** (2005) 16675–16680.
32. Ming Au, *Materials Science and Engineering B*, **117 (1)** (2005) 37–44.
33. T. Spassov, V. Rangelova, P. Solsona, M. D. Baro, D. Zander and U. Koster, *J. of Alloys and Compounds*, **398** (2005) 139–144.
34. X. Yao, C. Wu, A. Du, G. Qing Lu, H. Cheng, S. C. Smith, J. Zou and Y. He, *J. Phys. Chem. B*, **110** (2006) 11697–11703.
35. X. L. Wang, J. P. Tu, C. H. Wang, X. B. Zhang, C. P. Chen and X. B. Zhao, *J. of Power Sources*, **159 (1)** (2006) 163–166.
36. N. Hanada, T. Ichikawa and H. Fujii, *Physica B: Condensed Matter*, **383 (1)** (2006) 49–50.

37. L. Z. Ouyang, H. W. Dong, C. H. Peng, L. X. Sun and M. Zhu, *Int. J. of Hydrogen Energy*, **32 (16)** (2007) 3929–3935.
38. Z. Liu and Z. Lei, *J. of alloys and Compounds*, **443 (1–2)** (2007) 121–124.
39. Y. J. Choi, J. Lu, H. Y. Sohn and Z. Z. Fang, *J. of Power Sources*, **180** (2008) 491–497.
40. M. Lucaci, Al. R. Biris, R. L. Orban, G. B. Sbarcea and V. Tsakiris, *J. of Alloys and Compounds*, **488 (1)** (2009) 163–168.
41. M. G. Shelyapina, D. Fruchart and P. Wolfers, *Int. J. of Hydrogen Energy*, **35 (5)** (2010) 2025–2032.
42. S. Banerjee, C. G. S. Pillai and C. Majumder, *Int. J. of Hydrogen Energy*, **35 (6)** (2010) 2344–2350.
43. D. Dew–Hughes, *J. of Materials for Energy Systems*, **6 (4)** (1985) 239–241.
44. T. Sasai, K. Oku, H. Konno, K. Onouwe and S. Kashu, *J. of the Less Common Metals*, **89 (1)** (1983) 281–285.
45. M. Abdellaoui, D. Cracco and A. Percheron–Guegan, *J. of Alloys and Compounds*, **268** (1998) 233–240.
46. J. S. Han and J. Y. Lee, *J. of the Less–Common Metals*, **131** (1987) 109–116.
47. J. Chen, P. Yao, D. H. Bradhurst, S. X. Dou and H. K. Liu, *J. of Alloys and Compounds*, **293–295** (1999) 675–679.
48. R. Janot, L. Aymard, A. Rougier, G. A. Nazri and J. M. Tarascon, *J. of Physics and Chemistry of Solids*, **65** (2004) 529–534.
49. D. Shaltiel, *J. Less–Common Metals*, **62** (1978) 407–416.
50. S. Gulbrandsen–Dahl, Rapid Solidification of AB_5 Hydrogen Storage Alloys, *Ph. D. Dissertation*, NTN University, Norwegian (2002) 11–12.
51. F. Cuevas, J. M. Joubert, M. Latroche and A. Percheron–Guegan, *Applied Physics A*, **72** (2001) 225–238.
52. K. H. J. Busckow and H. H. Van Mal, *J. of the Less–Common Metals*, **29** (1972) 203–210.
53. L. Yan–jing, Z. Lei, C. Yan, C. Hu, J. Xu–yu, and W. Zhong, *Trans. Nonferrous Met. Soc. China*, **17** (2007) 978–984.
54. M. V. Ananth, M. Ganesan, N. G. Renganathan and S. Lakshmi, *Int. J. of Hydrogen Energy*, **34 (1)** (2009) 356–362.
55. Y. Zhang, M. Chen, X. Wang, G. Wang, X. Dong and Y. Qi, *Electrochimica Acta*, xxx (2003) xxx–xxx.

56. T. Nietsch, *Int. J. Hydrogen Energy,* **21** (1996) 984–991.
57. J. O. Hirshfelder, C. F. Curtis and R. B. Bird, Molecular Theory of Gases and Liquids (1954) *Wiley, New York*.
58. J. B. Jones and R. E. Dugan, Engineering Thermodynamics (1998) *Prentice–Hall of India, New Delhi*.
59. J. Bloch, *J. of Alloys and Compounds*, **312** (2000) 135–153.
60. J. Bloch and M. H. Mintz, *J. Alloys and Compounds*, **253–254** (1997) 529.
61. K. J. Laidler, Chemical Kinetics, *Pearson Education Pte. Ltd, India* (2004) 21–25.
62. H. S. Fogler, Elements of chemical reaction engineering, 558–587.
63. V. R. Subramanian, H. J. Ploehn and R. E. White, *J. of the Electro–chemical society*, **147 (8)** (2000) 2863–2873.
64. K. F. Kelton, *Materials Science and Engineering*, **A226–228** (1997) 142–150.
65. P. Muthukumar, A. Satheesh, M. Linder, R. Mertz and M. Groll, *Int. J. Hydrogen Energy*, **34** (2009) 7253–7262.
66. www.risoe.dk/rispubl/art/2006_15.pdf
67. M. T. Hagstrom, S. N. Klyamkin and P. D. Lund, *J. of Alloys and Compounds*, **293–295** (1999) 67–73.
68. C. Y. Seo, Z. L. Zhang, J. H. Kim, P. S. Lee and J. Y. Lee, *Int. J. of Metals and materials*, **8 (4**) (2002) 341–346.
69. T. Nietsch, *Int. J. Hydrogen Energy,* **21 (12)** (1996) 984–991.
70. J. Smith, H. Van Ness and M. Abbott, Introduction to Chemical Engineering Termodynamics, *Fifth Edition, McGraw–Hill* (1996).
71. www.waste.environment.vin.bg.ac.rs
72. S. Miao, Electronic structure and bonding in energy storage materials, *Ph. D. dissertation* (2007) California Institute of Technology, Pasadena, California.
73. www.en.wikipedia.org
74. E. Johansson, Synthesis and characterization of potential hydrogen storage materials, *Ph. D. dissertation* (2004) ACTA universitatis, Upsaliensis, Uppsala.
75. J. Kapischke and J. Hapke, *Experimental Thermal and Fluid Science*, **18** (1998) 70–81.
76. R. Gremaud, C. P. Broedersz, D. M. Borsa, A. Borgschulte, P. Mauron, H. Schreuders, J. H. Rector, B. Dam and R. Griessen, *Advanced Materials*, **19** (2007) 2813–2817.

77. F. S. Yang, G. X. Wang, Z. X. Zhang, X. Y. Meng and V. Rudolph, *Int. J. Hydrogen Energy*, **35** (2010) 3832–3840.
78. S. E. Guthrie, G. J. Thomas, W. Bauer and N. Y. C. Yang, The Development of Lightweight Hydride Alloys Based on Magnesium, *Sandia National Laboratories Report* (1996) SAND97–8220 UC-404.
79. G. Sandrock, *J. of Alloys and Compounds*, **295** (1999) 877–888.
80. Gavin Walker (Edited), Solid State Hydrogen Storage Materials, *Woodhead Publishing Limited, Cambridge – England* (2008) 357–375.
81. B. Bogdanovic, K. Bohmhammel, B. Christ, A. Reiser, K. Schlichte, R. Vehlen and U. Wolf, *J. of Alloys and Compounds*, **282** (1999) 84–92.